Endocannabinoids modulate cortical development by configuring Slit2/Robo1 signaling

Alán Alpár[a,§], **Giuseppe Tortoriello**[a], **Daniela Calvigioni**[a,b], **Micah J Niphakis**[c], **Ivan Milenkovic**[d], **Joanne Bakker**[b], **Gary A Cameron**[e], **János Hanics**[f], **Claudia V Morris**[g], **János Fuzik**[b], **Gabor G Kovacs**[d], **Benjamin F Cravatt**[c], **John G Parnavelas**[h], **William D Andrews**[h], **Yasmin L Hurd**[g], **Erik Keimpema**[a,b,#], and **Tibor Harkany**[a,b,#,*]

[a]Division of Molecular Neurobiology, Department of Medical Biochemistry & Biophysics, Scheeles väg 1:A1, Karolinska Institutet, SE-17177 Stockholm, Sweden

[b]Department of Molecular Neurosciences, Center for Brain Research, Medical University of Vienna, Spitalgasse 4, A-1090 Vienna, Austria

[c]Department of Chemical Physiology and The Skaggs Institute for Chemical Biology, The Scripps Research Institute, 10550 N. Torrey Pines Rd.,La Jolla, California CA 92037 USA

[d]Institute of Neurology, Medical University of Vienna, AKH 4J, Währinger Gürtel 18-20, A-1090 Vienna, Austria

[e]Institute of Medical Sciences, University of Aberdeen, Foresterhill, Aberdeen AB25 2ZD, United Kingdom

[f]Department of Anatomy, Histology and Embryology, Semmelweis University, T zoltó u. 58, H-1094 Budapest, Hungary

[g]Icahn School of Medicine at Mount Sinai, New York, 1470 Madison Avenue, New York, NY 10029, USA

[h]Department of Cell and Developmental Biology, 21 University Street, University College London, London WC1E 6DE, United Kingdom

Abstract

Local environmental cues are indispensable for axonal growth and guidance during brain circuit formation. Here, we combine genetic and pharmacological tools, as well as systems neuroanatomy

in human fetuses and mouse models, to study the role of endocannabinoid and Slit/Robo signaling in axonal growth. We show that excess 2-arachidonoylglycerol, an endocannabinoid affecting directional axonal growth, triggers corpus callosum enlargement due to errant CB_1 cannabinoid receptor (CB_1R)-containing corticofugal axon spreading. This phenotype mechanistically relies on the premature differentiation and end-feet proliferation of CB_2R-expressing oligodendrocytes. We further show the dependence of both axonal Robo1 positioning and oligodendroglial Slit2 production on cell-type specific cannabinoid receptor activation. Accordingly, Robo1 and/or Slit2 manipulation limits endocannabinoid modulation of axon guidance. We conclude that endocannabinoids can configure focal Slit2/Robo1 signaling to modulate directional axonal growth, which may provide a basis for understanding impaired brain wiring associated with metabolic deficits and prenatal drug exposure.

Keywords

Axon guidance; brain development; chemorepulsion; corticofugal axon

Axonal pathfinding decisions rely on short- and long-range intercellular cues determining cytoarchitectural arrangements permissive for directional growth in the developing brain. Guidance cues include a plethora of structurally heterogeneous proteins, released during defined temporal windows and acting within circumscribed spatial domains. Slits, a family of phylogenetically-conserved chemorepellent molecules[1], bind Roundabout (Robo)1/2 receptors[2,3] to regulate axonal tract formation during forebrain development[4-8]. Slit/Robo1/2 signaling is implicated in midline crossing[9-12] and the dorsoventral positioning of long-range axons[13,14], thus being indispensable for the basic forebrain wiring diagram and connectivity principles to emerge. Accordingly, Robo1$^{-/-}$ mice present the dysgenesis of major commissural tracts[5] and axon guidance errors in the corticofugal system[4]. Similarly, Slit2$^{-/-}$ and Slit1$^{-/-}$/Slit2$^{-/-}$ mice show corticothalamic and thalamocortical targeting defects[8], as well as optic tract abnormalities[12]. In addition, axons coalesce into enlarged fascicles in Robo1$^{-/-}$ mice[5]. Heparin sulphate proteoglycans and transcription factors, including members of the T-box or the LIM homeodomain families can influence Slit/ Robo1/2 signaling[14]. Nevertheless, the molecular identity of signaling networks for the upstream and local control of coordinated Slit/Robo1/2 expression, subcellular positioning and signal competence during corticogenesis remains relatively poorly explored.

Signaling lipids have recently emerged as regulators of neuronal development. Endocannabinoids, the natural ligands of cannabinoid receptors, modulate both neuronal[15] and glial[16] differentiation, and are efficacious to facilitate neurite extension and growth cone steering decisions[17-19]. CB_1 cannabinoid receptors (CB_1Rs) contribute to regulating the fasciculation and pallidal targeting of corticofugal axons[17]. In contrast, CB_2 cannabinoid receptors (CB_2Rs) are co-expressed with key enzymes of 2-arachidonoylglycerol (2-AG) metabolism in glia[20], and promote the differentiation of cultured oligodendrocytes[21], the cellular source of myelin sheaths in the nervous system[22].

Here, we show that pharmacological enhancement of 2-AG bioavailability during corticogenesis in mouse triggers the CB_2R-dependent differentiation of oligodendrocytes.

Premature oligodendrocyte end-feet proliferation *in vivo* coincides with CB_1R-dependent fasciculation errors of corticofugal projections, including altered axon bundle formation in the paramedian domain of the corpus callosum. We hypothesized that endocannabinoids, by simultaneously engaging cell-type specific cannabinoid receptors, might orchestrate chemorepulsion of cortical axons *via* a mechanism operating *in trans*, with oligodendrocytes producing surplus chemorepellents. By implementing a multi-parametric approach encompassing neuroanatomy in human and mouse fetuses, mRNA profiling, biochemistry, *in vitro* analysis and genetic models we identify oligodendrocyte-derived Slit2 acting at Robo1 receptors in corticofugal axons downstream from the respective activation of CB_2Rs and CB_1Rs upon pharmacological manipulation of 2-AG degradation as the molecular underpinning of endocannabinoid-induced corticofugal axon guidance errors. We find cannabinoid receptor activation to facilitate Slit2 accumulation in oligodendrocyte end-feet, and Robo1 accumulation in axonal growth cones. Overall, these data suggest that endocannabinoid signaling can regulate Slit/Robo interactions during the establishment of forebrain axonal tracts.

RESULTS

JZL184 increases 2-AG levels in fetal and adult cortices

To enhance endogenous 2-AG signaling in gravid mice we employed the small molecule JZL184 from embryonic day (E)12.5-18.5 to inhibit monoacylglycerol lipase (MGL), the enzyme chiefly responsible for degrading 2-AG in the nervous system[23]. The selective inhibition of MGL by JZL184 was confirmed with activity-based protein profiling of serine hydrolases in the brains of JZL184 and vehicle-treated dams and their E18.5 embryos. Consistent with previous reports[24], JZL184 displayed a high selectivity for MGL across all detectable brain serine hydrolases (Fig. 1a) leading to a significant increase in 2-AG levels in adult and embryonic cortices (Fig. 1b). While fatty-acid amide hydrolase (FAAH[25]), which catabolizes the endocannabinoid anandamide (AEA), was partially inhibited by JZL184 in adult and to a lesser degree, embryonic brain samples, we did not observe a significant increase in AEA levels in fetal or adult cortices (Fig. 1b). The levels of 2-linoleoyl glycerol (2-LG; a congener of 2-AG) and oleoylethanolamide (OEA; an analogue of AEA), were both unaffected by JZL184 treatment (Fig. 1b). Together, these data confirm that JZL184 selectively targets MGL leading to an accumulation of 2-AG in the brains of gravid adult mice and their offspring.

MGL inhibition induces axon fasciculation deficits

We studied the morphology of corticofugal axons in developing fetal brains after JZL184 exposure, since these tracts contain the highest levels of CB_1Rs during embryonic development[18]. JZL184 exposure induced L1 neural cell adhesion molecule (L1-NCAM)$^+$ axons to coalesce into enlarged fascicules (Fig. 2a,b, Supplementary Table I) irrespective of the rostrocaudal axis of the developing brain (Supplementary Fig. 1a-c). The enlarged axon fascicles were found spread in the cortical plate, including intermediate zone (IZ) territories otherwise devoid of L1-NCAM$^+$ processes (Fig. 2i,j; Supplementary Fig. 1a).

The coalescing of axonal fibers upon JZL184 exposure was altered irrespective of their origin or projection targets. In particular, enlarged fascicles were observed to cross the midline (Fig. 2e,f), populated the suprastriatal domain of the corpus callosum (Fig. 2m,n, Supplementary Fig. 2a) or invaded the striatum (Fig. 2o,p). Both corticothalamic and thalamocortical axons were affected in the striatum, as revealed by TAG-1[26,27] and CTFL[17] immunohistochemistry, respectively (Supplementary Fig. 2a-e,r). These findings suggest the multimodal interplay of corticofugal and thalamocortical projections along their reciprocal growth paths during the mechanism termed axonal "handshake"[28].

Next, we examined mice carrying GFP-tagged cytosolic tau in neurons[29] in the presence or absence of CB_1Rs ($tau^{gfp/gfp}::CB_1R$)[29] to show that radial glia ($RC2^+$) fibers and postmitotic $Brn1^+$ pyramidal cells[16] arranged perpendicular to corticofugal axons and adopted alternative paths (Fig. 2i,j). We then administered JZL184 to $CB_1R^{-/-}$ fetuses to test the reliance of pharmacologically-induced axon guidance errors on CB_1Rs, selectively localized to the corticofugal system by mid-gestation[18]. In accord with previous reports[18,30], CB_1R deletion alone induced axon fascicle enlargement (Fig. 2c,g,k,q). In $CB_1R^{-/-}$ animals, JZL184 did not affect the diameter of first-order fascicles (18.78 ± 1.66 μm [JZL184] *vs.* 16.04 ± 1.28 μm [vehicle] (mean $\pm$ s.e.m.; $n = 3$ mice per group); Fig. 2d,h and q). $CB_1R^{-/-}$ mice treated with JZL184 presented significantly increased axon spreading in the IZ/corpus callosum (203.81 ± 8.44 μm [JZL184] *vs.* 157.27 ± 6.28 μm [vehicle], $n = 3$ mice per group, $p < 0.05$ (Student's *t*-test); Fig. 2q). This was associated with altered distribution of radial glia processes and $Brn1^+$ pyramidal cell radially migrating towards the cortical plate – to avoid axon-packed microdomains – in $tau^{gfp/gfp}::CB_1R^{-/-}$ reporter mice (Fig. 2l).

The dynamic control of axonal growth and fasciculation involves the elimination of functionally-redundant or mistargeted processes over time. Mature axons become embedded in extracellular matrix, a three-dimensional scaffold of molecularly heterogeneous proteins [31] to maintain their positions in axon fascicles. Here, we find that neurocan, a chondroitin sulfate proteoglycan whose expression is essential for cell adhesion and slows neurite extension [32], is excluded from enlarged axonal fascicles upon JZL184 treatment (Fig. 2m-p) suggesting altered neurite motility and pathfinding. The JZL184-induced remodeling of the corticofugal system also impacted the coincident patterning of thalamocortical afferents (Supplementary Fig. 2a-e), robustly affecting their "handshake"[28].

Nevertheless, the JZL184-induced axonal phenotype was absent in constitutive $MGL^{-/-}$ mice (Supplementary Fig. 3). Chronic 2-AG signaling in $MGL^{-/-}$ mice is characterized by CB_1R down-regulation and desensitization, suggesting compensation for increased CB_1R signaling events[23]. Inhibition of MGL by JZL84 in our experimental model (E12.5-E18.5) would likely induce excessive CB_1R signaling, resulting in physiological alterations otherwise compensated for in $MGL^{-/-}$ mice. Thus, we conclude that excess 2-AG availability brought about by the pharmacological disruption of their degradation during defined periods of corticogenesis is sufficient to remodel the corticofugal projection system.

Unchanged CB_1R signal transduction upon JZL184 exposure

Repeated JZL184 administration can induce cannabinoid receptor desensitization and functional antagonism[23]. Therefore, we first sampled mRNA (Supplementary Table II) and

protein expression of molecular constituents of the 2-AG signaling cassette (Fig. 2s, Supplementary Fig. 4). Neither mRNA nor protein levels for *sn*-1-diacylglycerol lipases α and β (DAGL), synthesizing 2-AG[33], MGL and ABHD6, involved in 2-AG degradation[34,35], and CB_1Rs changed significantly in JZL184-exposed fetal cortices (Supplementary Fig. 4a,b). We then used extracellular signal regulated kinase 1/2 (Erk1/2) phosphorylation as read-out[36] upon acute agonist challenge (WIN55,212-2, 100 nM) of cultured cortical neurons pre-treated with JZL184 for 4 days to address whether JZL184 induced CB_1R desensitization. JZL184 alone did not induce constitutive Erk1/2 phosphorylation, and AM 251, a CB_1R antagonist, did not modify JZL184 effects. Notably, JZL184 allowed WIN55,212-2-induced rapid Erk1/2 phosphorylation (Fig. 2t,u) with comparable temporal dynamics to that in control (Supplementary Fig. 4c), which is compatible with earlier data showing that only prolonged (> 8 days) agonist stimulation induces CB_1R desensitization *in vitro*[36]. These data suggest that supra-physiological 2-AG signals upon JZL184 application during corticogenesis alter axon fasciculation *via* neuronal CB_1Rs, while a non-CB_1R-mediated mechanism might account for the increased axonal spread in the prospective corpus callosum.

Oligodendrocyte end-feet proliferate among misrouted axons

Excessive spreading of corticofugal axons committed to the prospective corpus callosum in JZL184-treated $CB_1R^{-/-}$ mice led us to hypothesize that a CB_1R-independent mechanism can alter the pathfinding of corticofugal axons. Therefore, we tested whether premature differentiation of oligodendrocytes, which postnatally produce myelin to ensheath callosal axons[22] and co-express CB_1Rs and CB_2Rs[20], could participate in axonal misrouting. JZL184 facilitated the accumulation of oligodendrocytes that expressed 2′,3′-cyclic-nucleotide 3′-phosphodiesterase (CNPase)[20], and formed micro-islands interspersed with corticofugal axons in both wild-type and $CB_1R^{-/-}$ mice (Fig. 3a-d). Oligodendrocyte differentiation was reflected by the increased density (Fig. 3e) and size (Fig. 3f) of their CNPase[+] end-feet targeted towards nearby axons. The JZL184-induced morphogenesis of oligodendrocytes was CB_1R independent since it also occurred in $CB_1R^{-/-}$ mice (density: 37. 7 ± 3.1 [JZL184] *vs*. 14.7 ± 2.7 [vehicle] end-feet/1,000 μm^2, *p* < 0.05; Fig. 3e). By Western blotting, we quantitatively confirmed that JZL184 significantly elevated CNPase and myelin basic protein (MBP) levels in the fetal cerebrum (Fig. 3g,h). These results outline a multicomponent mechanism with 2-AG simultaneously activating CB_1Rs in axons and CB_2Rs in oligodendrocytes in JZL184-exposed fetuses. Nevertheless, a causal relationship between altered axonal navigation and glial proliferation remains unknown. Here, we reasoned that endocannabinoid-induced glial differentiation might instruct the production of a chemorepellent for the focal remodeling of the corticofugal tract (Fig. 3i).

CB_1Rs co-exist with Robo1/2 receptors in corticofugal axons

Neurons and glia interact to form chemical conduits for axonal growth during brain development[14]. Slit/Robo interplay is fundamental for the development of major axonal tracts, including corticofugal projections[4,5], with midline glia being a primary source of chemorepellent Slit1/2[37]. However, the upstream regulation of Slit/Robo signaling in axon guidance is not entirely understood. We hypothesized that endocannabinoid-induced oligodendroglia positioning and differentiation in conjunction with 2-AG's cell-type specific

action *via* CB_1Rs and CB_2Rs could orchestrate *in trans* Slit/Robo signaling. Therefore, we first examined whether CB_1Rs and Robo1 receptors co-exist in long-range axons. By using serial sections from human fetuses at gestational weeks 20-23 (Supplementary Table III), we find the expression patterns of CB_1Rs and Robo1 receptors to overlap in forebrain axonal tracts, particularly axons coursing in the internal capsule (Fig. 4a-d). Multiple immunofluorescence labeling substantiated that CB_1Rs and Robo1 receptors indeed co-distributed along the same axons in humans (Fig. 4e-g). Likewise, corticofugal axons in the E18.5 fetal mouse brain contained both receptors (Fig. 4h-m). In addition, CB_1R^+ cortical axons in the corpus callosum harbored Robo2 receptors (Fig. 4n-p).

Robo1 accumulates in JZL184-exposed neuronal growth cones

Axonal growth is a dynamic process, with growth cones continuously sampling the local microenvironment and responding to chemotactic cues by initiating turning decisions[38]. Robo1/2 localization to growth cones underpins Slit/Robo signaling during axonal pathfinding[13,39]. Based on our pharmacological data (Supplementary Fig. 4d), we hypothesized that modifications to axonal growth trajectories might be mediated by the CB_1R-dependent repartitioning of Robo1 receptors in axonal growth cones. Therefore, we confirmed the co-localization of CB_1Rs and Robo1 receptors *in vitro* (Fig. 5a), and validated Robo1/2 mRNA and protein expression by PCR (Fig. 5b) and Western blotting (Fig. 5c). Upon JZL184 treatment of cultured cortical neurons, Robo1 receptors accumulated in growth cones, specified as the fluorescence ratio between the growth cone and adjoining neurite shaft (Fig. 5d). This response was O-2050 sensitive[30], confirming CB_1R involvement. In contrast, Robo2 receptor distribution remained unchanged (Fig. 5e). We also found a decreased co-localization coefficient for Robo1 and CB_1R, reinforcing increased Robo1 receptor import if CB_1R levels remained stationary and partition separately from Robo1 (Fig. 5f, Supplementary Fig. 5a). Next, we purified growth cone particles (GCPs)[19] from fetal mouse cortices treated *en-block* with JZL184 (100 nM) up to 80 min to highlight the *in vivo* relevance of our findings. Robo1 receptor accumulated in JZL184-exposed GCPs (Fig. 5g), lending further support to the concept that superfluous 2-AG signaling can redistribute Robo1 receptors in a CB_1R-dependent fashion. Furthermore, we suggest that axonal transport contributes to Robo1 accumulation in growth cones, since we detected a JZL184-induced increase in Robo1 receptor immunofluorescence in the distal (presumed motile)[30] part of the neurite adjacent to the growth cone (Fig. 5h).

JZL184-induced alterations in Robo1 but not Robo2 protein expression were rescued by OMDM188, an inhibitor of DAGLs producing 2-AG[40], implicating 2-AG dependence of Robo1 signaling (Supplementary Fig. 4d,e). Therefore, we focused on the endocannabinoid-dependence of Slit2/Robo1 interactions.

To confirm the reliance of our proposed mechanism on MGL activity, we transfected primary cortical neurons with MGL siRNA and assessed Robo1 receptor intensity in the growth cone. Transient MGL knock-down recapitulated the accumulation of Robo1 immunoreactivity within the growth cone (Fig. 5i,j, Supplementary Fig. 5d,e), which was CB_1R dependent given its sensitivity to AM251, a CB_1R inverse agonist (Fig. 5k). In addition, the lack of Robo1 receptor responsiveness in the growth cones of primary cortical

cultures from $CB_1R^{-/-}$ mice reinforced the critical involvement of CB_1Rs in this regulatory process (Fig. 5i-n). CB_1R activation in developing neurons triggers molecularly diverse second messenger cascades[41]. Here, we found that JZL184-induced Robo1 receptor accumulation in growth cones was occluded by the administration of both UO126 and SP600125, MEK1/2 and JNK inhibitors, respectively (Fig. 5o, p).

If a CB_1R-mediated increase of Robo1 signaling is of pathophysiological significance then Robo/Slit mRNA levels might be expected to coordinately change in the cortices of human fetal subjects exposed *in utero* to cannabis, relative to controls. By using NanoString technology (Supplementary Table IV), we found that Robo1 receptor mRNA expression tended to be significantly higher in cannabis-exposed subjects ($F_{1,26} = 4.156$; $p = 0.056$; Supplementary Fig. 1d). This change was driven by a significant impact of developmental growth measures. Similarly for Slit1 mRNA, there was a significant confound of development resulting in only a trend effect ($p = 0.093$) for the contribution of cannabis exposure. Interestingly, there was a significant correlation ($r = 0.576$; $p = 0.002$) between the expression of Robo1 and Slit1 mRNAs in the human fetal cortex suggesting a functional interaction irrespective of cannabis predisposition.

JZL184 promotes Slit2 production in oligodendrocytes

Genetic deletion of Slit1 and/or Slit2 induces midline crossing errors[8,12]. Therefore, we hypothesized that oligodendrocytes could produce excess Slits in a CB_2R-dependent fashion to impact corticofugal axon fasciculation. Due to methodological constraints to histochemically detect Slit1, we adopted a candidate approach and focused on Slit2 throughout our proof-of-concept experiments. We first prepared oligodendrocyte cultures, which only sporadically contained astroglia (Fig. 6a) to demonstrate that CNPase[+] oligodendrocytes are a likely source of Slit2 *in vitro*. We extended these data by comparing glial fibrillary acidic protein (GFAP)[+] astroglia and oligodendroglia cultures (Fig. 6b) and showing that oligodendroglia selectively contain detectable Slit2 mRNA transcripts and Slit2-like protein (Fig. 6c, Supplementary Fig. 5b, 6). Slit2-like immunoreactivity was seen only in oligodendrocytes (but not astroglia or neurons; Fig. 6a) *in vitro* and mainly localized to their soma (Fig. 6d) and membranes of their processes (Fig. 6e,f). We confirmed our Slit2 detection in oligodendrocytes by demonstrating significant diminished Slit2-like content in oligodendroglia from $Slit2^{-/-}$ mice (Supplementary Fig. 6a-e). Additionally, we validated our staining protocols by co-labeling for an antibody revealing a phylogenetically conserved sequence from the *Drosophila* Slit ortholog (Fig. 6c). These data identify oligodendrocytes as a candidate source of Slit2.

Excess 2-AG facilitates oligodendrocyte differentiation in culture[21] and *in vivo* (Fig. 3). Here, we show that JZL184 increased Slit2 expression in cultured oligodendrocytes (Fig. 6g-i), and increased Slit2-like immunoreactivity in their end-feet (Fig. 6j). JZL184's effect on Slit2-like labeling in oligodendroglia end-feet was reversed by AM630, a CB_2R antagonist[21] (Fig. 6k-m), suggesting that Slit2 production and subcellular translocation might be regulated by agonist (e.g., 2-AG) signaling at CB_2Rs. To verify the effects of JZL184 on Slit2 production, we transfected cultured oligodendrocytes with MGL siRNA,

which recapitulated the increase of Slit2-like immunoreactivity in oligodendrocyte end-feet (Fig. 6o,p).

In JZL184-treated brains, CNPase$^+$/CB$_1$R$^-$ oligodendroglial end-feet juxtaposed Robo1/CB$_1$R double-labeled corticofugal axons (Fig. 6q), and accommodated enlarged fascicles by forming proportionately larger glial scaffolds (that is, no CNPase labeling within individual fascicles; Fig. 6q). These oligodendroglia end-feet harbored Slit2-like immunoreactivity, which frequently juxtaposed nearby axons (Fig. 6r). These data together with Robo1/CB$_1$R (Fig. 5a) and Robo2/CB$_1$R (Fig. 5a) co-localization and Robo1/Robo2 mRNA (Fig. 5b) and protein (Fig. 5c) expression in cultured cortical neurons suggest that endocannabinoids are poised to modulate Slit/Robo signaling, and support a model in which ectopic Slit2 presentation by cortical oligodendrocytes participates in inducing growth errors of CB$_1$R$^+$ axons *in vivo* (Fig. 6s).

JZL184 fails to affect axonal growth in Robo1$^{-/-}$ mice

If focal Robo1/Slit2 interactions are indeed modulated by 2-AG signaling then JZL184 administration to Robo1$^{-/-}$[42] mice will reveal incomplete cortical phenotypes due to the neuron *vs*. oligodendroglia-driven arch of the proposed signaling axis (Fig. 7a). Robo1$^{-/-}$ mice *per se* present an axon fasciculation phenotype[5]. If Robo1 receptors are downstream from CB$_1$Rs, then JZL184 likely would fail to affect the pre-existing axonal phenotype in Robo1$^{-/-}$ mice. Indeed, the spread of callosal axons[5] (Fig. 7b) remained unaffected in JZL184-treated Robo1$^{-/-}$ mice. As such, neither the diameter of individual and enlarged axon fascicles nor their interbundle distance were affected by JZL184 (Fig. 7c,d,f). In contrast, JZL184 provoked CNPase$^+$ oligodendroglial end-feet differentiation in Robo1$^{-/-}$ mice. Yet oligodendroglial end-feet were interspersed with individual corticofugal axons, confirming the loss of a chemorepulsive cue (Fig. 7e,g). These data dissociate between the loss of CB$_1$R-driven and Robo1 receptor-dependent axon guidance deficits and CB$_2$R-mediated focal chemorepulsion and oligodendroglial differentiation *in vivo*.

Slit2/Robo1 signals mediate JZL184-induced chemorepulsion

We devised a genetically amenable co-culture system to show that Slit2$^+$ oligodendrocytes affect directional growth decisions of Robo1$^+$/CB$_1$R$^+$ neurites *in vitro*. Neurites regularly contacted oligodendrocytes under control conditions (Fig. 8a). JZL184 administration *in vitro* enhanced Slit2 expression and mobilized Slit2 to submembranous positions in oligodendrocytes (Fig. 8b) with coincident repulsive responses of nearby neurites as shown by their increased distance to apposing glial surfaces (15.65 ± 1.01 μm [JZL184] *vs*. 9.74 ± 1.11 μm [vehicle], $p < 0.05$; Fig. 8d).

We used siRNA knockdown of Robo1 in neurons co-cultured with oligodendrocytes in the presence of JZL184 for 4 days to test whether JZL184-mediated neurite repulsion relied on Robo1 receptors. Co-transfection with a GFP-plasmid and *post-hoc* labeling for Robo1 receptors (Supplementary Fig. 5c) confirmed successful neuronal Robo1 silencing. Robo1 knockdown overcame JZL184-induced repulsion and adopted differentiated growth cone morphologies (Fig. 8c). Consequently, neurites of Robo1 siRNA-transfected neurons approached oligodendrocytes, leaving the growth cone-oligodendrocyte distance

significantly reduced (4.97 ± 0.69 μm [Robo1 siRNA] *vs.* 18.21 ± 2.06 μm [scrambled siRNA], $p < 0.05$; Fig. 8d). Further, JZL184 administration increased the number of branching points on approaching neurites in the close vicinity of oligodendocytes (Fig. 8e), suggesting that an increased number of axon collaterals might, at least in part, contribute to changes in callosal microanatomy. Cumulatively, these data identify endocannabinoids as candidates to upstream regulate Slit2/Robo1 interactions during directional axonal growth (Fig. 8f,g).

DISCUSSION

Endocannabinoids affect neuronal differentiation, including directional axonal growth during corticogenesis[17,19,43]. Endocannabinoid signaling appears particularly efficacious to modulate axonal growth since CB_1Rs are selectively enriched in navigating axons, and are co-targeted with DAGLs to advancing growth cones[30,43]. Establishment of major axonal tracts critically relies on chemorepulsive Slit gradients[4,5,7]. In fact, midline crossing of commissural axons particularly depends on focal Slit/Robo signaling between neurons and glia[44]. The architecture of corticofugal axons is altered in $CB_1R^{-/-}$ mice[18], a phenotype reminiscent to those of Robo1$^{-/-}$/Robo2$^{-/-}$ mutants[4]. Here, we resolve this similarity by dissecting a molecular interplay between endocannabinoids and the Slit/Robo signaling axis. Our data suggest that the lack of CB_1R-induced Robo1 accumulation in growth cones might disrupt, at least in part, axonal navigation and contribute to the altered topography of corticofugal axons in $CB_1R^{-/-}$ mice. However, by showing that increased 2-AG levels upon MGL inhibition coincidently induce CB_2R-mediated oligodendrocyte differentiation and CB_1R-dependent axonal misrouting in the corpus callosum, we characterize an intercellular signaling network in which a single endocannabinoid ligand engages molecularly distinct cannabinoid receptors in neurons and glia to upstream control chemorepellent production (Slit2 in glia) and signaling (Robo1 in neurons). Whether changes in axonal topography in the corpus callosum of JZL184-treated mice reflect an increased number of axon collaterals or instead are due to the spatial reorganization of the same number of axons (because of, e.g., changes to extracellular matrix composition) as in controls remains unknown. Our *in vitro* data on the JZL184-induced increase of neurite branching points supports the former scenario, and suggests that an increased numbers of axon collaterals compacting in callosal fascicles might significantly increase network instability due to erroneous synaptic wiring. Our results in cultured neurons are also compatible with those from Robo1$^{-/-}$ mutant embryos where glial re-positioning around enlarged axon fascicles could argue for the disruption of a critical glial-neuronal signal interface.

We employed JZL184, a selective MGL inhibitor[23], to increase endocannabinoid levels in the fetal brain. The selectivity of this compound was verified using activity-based protein profiling after *in vivo* drug application, as well as in *in vitro* experiments using genetically or RNA silenced primary cultures. Since JZL184 application does not desensitize CB_1R unless used for extended periods[36], our data suggest that ectopic, cell type- and cannabinoid receptor subtype-dependent signaling events took place in JZL184-exposed fetuses, sufficient to affect axonal growth and guidance. This included an increased transport of Robo1 along the axon culminating in peak expression levels and externalization in the growth cone, likely modulated *via* MAPK and JNK signaling, as well as an increased Slit2

expression on an enlarged oligodendroglial end-feet arbor. Considering that CB_1Rs are broadly distributed in the developing nervous system[45,46], including descending projections to the spinal cord[45,47], our results might have profound implications for the overall organization of axonal connectivity in the nervous system.

Although we did not seek to identify the cellular origin of signal-competent 2-AG, a number of alternative sources may exist. These include the elongating corticofugal axons themselves, which contain DAGLα (and β)[17,18]. If so, Slit2/Robo1 signaling might represent a cell-autonomous amplification mechanism whereby DAGL-derived 2-AG could activate CB_1Rs within growth cones[30], facilitating Robo1 trafficking. Recent data suggest that 2-AG can diffuse extracellularly and evoke physiological responses in a radius of 20-100 μm[48,49]. Thus, DAGL activity in axonal growth cones appears sufficient to generate focal 2-AG microgradients to activate CB_2Rs on neighboring oligodendrocytes to stimulate Slit2 production and release (Fig. 8f,g). At the level of signal transduction, CB_1Rs and Robo1/2 can coordinately activate downstream effectors within axonal growth cones, which can act as reinforcers of the individual receptors' signal outputs. Members of the Rho family of GTPases, which can be activated by either receptor in various tissues[19,50,51] and whose activity is indispensable for cytoskeletal instability allowing growth cone motility[52], can be central to orchestrating endocannabinoid-induced modifications to cytoskeletal remodeling during repulsive growth cone turning. An advantage of this model, combining elements of autocrine endocannabinoid and paracrine Slit2/Robo1 signaling, is that it ascertains the "on-demand" upstream coupling of endocannabinoids to Slit2/Robo1 signaling, outlining a temporally defined, spatially restricted and highly dynamic mechanism to modulate growth cone steering decisions.

We also show that CB_1R-Robo1 receptor co-localization is preserved during mammalian evolution, as evidenced by our histochemical data from mid-gestational human fetuses. Moreover, Robo1 and Slit mRNA expression in human fetal brains are developmentally regulated and appear tightly coupled. Maternal cannabis smoking significantly increased the amount of Robo1 mRNA in the human fetal cerebrum. We propose that the molecular re-configuration of Slit/Robo signaling networks by phytocannabinoids *via* the CB_1R can be a candidate molecular mechanism to explain altered synaptic neurotransmission, and consequently, behavioral and cognitive deficits in children exposed *in utero* to cannabis[53,54]. Considering the continued increase of cannabis smoking during adolescence[55], the erroneous recruitment of spatially segregated CB_1Rs and CB_2Rs to regulate Slit2/Robo1 interactions during the postnatal refinement of neuronal circuits might also introduce unwanted modifications to the cortical wiring diagram. Besides cannabis, fetal infections are associated with the induction of endocannabinoid signaling in placental macrophages, contributing excess endocannabinoids to the fetal circulation[56]. This cascade can change the temporal and subcellular recruitment of CB_1Rs and CB_2Rs, imposing pathological challenges on the signaling mechanism we uncovered. Overall, we suggest that a hierarchical interplay between endocannabinoid and Slit/Robo signaling networks is a primary regulatory node in the developing corticofugal system.

METHODS

Animals and tissue preparation

Tau$^{gfp/gfp}$::CB$_1$R$^{-/-}$ mice were generated by first crossing tau$^{gfp/+}$ and CB$_1$R$^{-/+}$ mice (both on C57BL/6 background) to select tau$^{gfp/+}$::CB$_1$R$^{-/+}$ colony founders. Next, we crossed heterozygous offspring to generate tau$^{gfp/gfp}$::CB$_1$R$^{-/+}$ parents for *in vivo* analysis. Given that tau is dispensable for neuronal development, tau$^{gfp/gfp}$ mice did not carry any developmental abnormality[29]. We used mice heterozygous for CB$_1$Rs as parents throughout the experiments, allowing direct comparison of littermate tau$^{gfp/gfp}$::CB$_1$R$^{-/-}$ and tau$^{gfp/gfp}$::CB$_1$R$^{+/+}$ offspring. MGL$^{+/+}$ and MGL$^{-/-}$ littermates of both sexes from heterozygous pregnancies[23] were analyzed on E16 and postnatal day (P)20 (Supplementary Fig. 1). Pregnant CB$_1$R$^{-/+}$, tau$^{gfp/gfp}$::CB$_1$R$^{-/+}$, Robo1$^{-/+}$[5], Slit2$^{+/-}$[57] and wild-type C57BL/6 mice were injected with JZL184 (40 mg/kg body weight, i.p. daily)[24] or vehicle intraperitoneally during E12.5-18.5. *Male* mouse embryos ($n > 6$/pregnancy, $n > 2$ pregnancies/analysis) were collected at E18.5. Whole brains were collected for histochemistry, protein biochemistry/Western blotting, mass spectrometry, JZL184 binding assay or quantitative RNA profiling. Experiments on live animals conformed to the 86/609/EEC directive and were approved by the regional authority (Stockholm Norra Djuretiska Nämnd; N512/12).

Human fetal tissue preparation and histochemistry

Three fetal brains with normal development (between 20-23 gestational weeks) were selected from the Brain Bank of the Institute of Neurology, Medical University of Vienna, Austria. Fetal brain tissue was obtained from spontaneous or medically induced abortions. Only cases without genetic disorders, head injury, or neurological diseases were included. These cases showed no chromosome aberrations or *post-mortem* autolysis. Neuropathological examination excluded major CNS malformations, severe hypoxic/ischemic encephalopathy, intraventricular hemorrhages, severe hydrocephalus and meningitis or ventriculitis. Demographic data were summarized in Supplementary Table III. Tissues were obtained and used compliant with the Declaration of Helsinki and following institutional guidelines. The study was performed in the course of an approved study by the Ethical Committee of the Medical University of Vienna (Nr.104/2009).

Immunohistochemistry, imaging and quantitative morphometry

Embryonic brains were immersion fixed in 4% paraformaldehyde in phosphate buffer (0.1 M, pH 7.4, PB) overnight. Tissue samples were cryoprotected in 30% sucrose in physiological saline for at least 48h before cryostat serial sectioning (16 μm thickness), and thaw-mounted on SuperFrost$^+$ glass slides. Multiple immunofluorescence histochemistry was carried out according to published protocols[19,58]. Sections were washed in PB and pre-treated with 0.3% Triton-X-100 (in PB) for 1h at 22 - 24 °C to enhance the penetration of primary antibodies. Non-specific immunoreactivity was suppressed by incubating our specimens in a cocktail of 10% normal donkey serum (NDS; Jackson), 5% bovine serum albumin (BSA; Sigma) and 0.3% Triton X-100 (Sigma) in PB for 1h at 22 - 24 °C. Sections were exposed (16 - 72h at 4 °C) to select combinations of primary antibodies (Supplementary Table I) diluted in PB to which 0.1% NDS and 0.3% Triton X-100 had been

added. After extensive rinsing in PB, immunoreactivities were revealed by carbocyanine (Cy)2, 3 or 5-tagged secondary antibodies raised in donkey (1:300 [Jackson], 2h at 22 - 24 °C). Hoechst 33,342 (Sigma), a nuclear dye, was applied to reveal tissue architecture. Sections were coverslipped with Dako Fluorescent mounting medium (Dako).

Sections were inspected and images acquired on a 710LSM confocal laser-scanning microscope (Zeiss). Image surveys were generated using the tile scan function at 10× primary magnification (Plan-Neofluar 10×/0.30). High-resolution images were acquired with optical zoom ranging from 1.5-3.0× at 63× primary magnification (Plan-Apochromat 63×/1.40, and 0.5-0.7 μm optical slice thickness) to limit signal detection. Emission spectra for each dye were limited as follows: Cy2 (505-530 nm), Cy3 (560-610 nm) and Cy5 (650-720 nm). The co-existence of immunosignals was verified by capturing serial orthogonal z image stacks at 63× primary magnification (up to 3× optical zoom) and accepted if these were present without physical signal separation in 1.0-μm optical slices, and overlapped in all three (x, y and z) dimensions within individual cellular domains.

Morphometric analysis of fetal mouse brains was aided by the ZEN2010 software and included: i) the transverse diameter (μm) of L1-NCAM$^+$ corticofugal axons ("*corpus callosum spread*") in fetal wild-type and $CB_1R^{-/-}$ and $MGL^{-/-}$ brains after JZL184 or vehicle administration, ii) the density and iii) proximity (μm) of first-order fascicles of > 3 μm in diameter, iv) the density (n) and v) diameter (μm) and vi) embedding of CNPase$^+$ oligodendrocyte end-feet interspersing callosal axons, and vi) calibrated fluorescence intensities using an arbitrary grey-scaled unit scale in images acquired with identical laser illumination and capture settings. Robo1 receptor immunoreactivity along growth cones and axons of primary cortical neurons was measured in ImageJ 1.45s (NIH). Validation of the Slit2 antibody was performed on 600 nm thin serial optical slices of embryonic brain sections obtained from Slit2$^{-/-}$ and littermate wild-type mice. The number of Slit2$^+$ profiles was counted and their density calculated on CNPase$^+$ oligodendrocyte end-feet or perinuclear loci. Multi-panel images were assembled in CorelDraw ×5.

Human fetal immunohistochemistry and analysis

Three-μm tissue sections of formalin fixed, paraffin-embedded tissue blocks containing the corpus callosum and the hippocampal formation were mounted on pre-coated glass slides (Star Frost)[59,60]. Shortly, after deparaffinization and rehydration, the sections were pre-treated in low pH EnVision FLEX antigen retrieval solution at 98 °C for 20 min (PTLink; Dako) and subsequently incubated with rabbit anti-Robo1 (ab7279; Abcam; 1:500) or guinea pig anti-CB_1R (Dr. M. Watanabe 1:1000) antibodies. The DAKO EnVision detection kit, peroxidase/DAB, rabbit/mouse (K5007, ready-to-use, Dako) was used to visualize antibody binding. Sections were counterstained with hematoxylin, dehydrated in ascending concentrations of ethanol, cleared with xylene and covered with Consil-Mount (Shandon; Thermo Scientific). Representative images containing the area of interest were exported from scanned sections (NanoZoomer 2.0, Hamamatsu).

For immunofluorescent co-localizations, 5 μm-thick sections were pre-treated with 1% sodium-borohydride, rinsed extensively in 25 mM Tris-Buffer (pH 7.5) and blocked in 20% normal horse serum (Vector Laboratories) for 30 min. Mixtures of primary antibodies were

applied for 48h at 4 °C (anti-Robo1 diluted 1:500 and anti-CB$_1$R diluted 1:1000). A mix of secondary antibodies conjugated with Alexa Fluor 488 (Invitrogen/Molecular Probes; 1:1000) and DyLight 650 (Jackson; 1:400) was applied for 2h at room temperature. The antibodies were tested for optimal dilution, and secondary antibodies were tested for cross-reactivity and non-specific staining. Sections were imaged and analysed using a Zeiss LSM780 confocal microscope.

Western blotting

Tissue samples were lysed in modified radioimmunoprecipitation assay buffer containing 1 mM NaF, 1 mM Na$_3$VO$_4$, 0.1% N-octyl-β-D-glucopyranoside, and a mixture of protease inhibitors (Complete, Roche). Cell debris and nuclei were pelleted by centrifugation (800 *g*, 10 min at 4 °C). Protein concentrations were determined by Bradford's colorimetric method[61]. Samples were diluted to a final protein concentration of 2 μg/μl, denatured in 5× Laemmli buffer, and analyzed by SDS-PAGE on 6% or 8% resolving gels. After transferring onto Immobilon-FL polyvinylidene difluoride membranes (Millipore), membrane-bound protein samples were blocked in 3% BSA and 0.5% Tween-20 diluted in Tris-buffered saline (TBS) for 1.5h, and subsequently exposed to primary antibodies (Supplementary Table I; Supplementary Fig. 7) overnight at 4 °C. Appropriate combinations of HRP-conjugated secondary antibodies (Jackson; from goat, rabbit, guinea pig or mouse hosts; 1:10,000 for 2h) were used for enhanced chemiluminescence signal detection. Image acquisition and analysis were performed on a Bio-Rad XRS$^+$ imaging platform. TUJ1 served as loading control which showed corresponding quantities of β-actin and gapdh (Supplementary Fig. 4f).

Polymerase chain reaction

To discriminate the sex of mouse fetuses, we used primers to amplify Y and X chromosome-specific genomic DNA sequences. The *Sry* gene (*forward*: GTTCAGCCCTACAGCCACAT, *reverse*: CAGCTGCTTGCTGATCTCTG, amplicon size: 197 bp [Y chromosome]) and *DXNds3* microsatellite (*forward*: GAGTGCCTCATCTATACTTACAG, *reverse*: TCTAGTTCATTGTTGATTAGTTGC, amplicon size: 244 bp [X chromosome]) were amplified. For quantitative PCR, E18 embryonic mouse brains were microdissected on ice to isolate pallial regions and snap frozen in liquid N$_2$ until processing. RNA was extracted using the RNeasy mini kit (Qiagen) with a DNase I step performed to eliminate traces of genomic DNA[30] and reverse transcribed using a high-capacity cDNA reverse transcription kit (Applied Biosystems). Reactions were performed after an initial denaturation at 95 °C for 10 min followed by 40 cycles of 95 °C for 15 s denaturation, annealing and extension at calculated temperatures (60 s), and a dissociation stage (from 60 to 95 °C with 0.5 °C steps for 10 s each; MyiQ Apparatus, Bio-Rad), with primer pairs amplifying short fragments for each gene (Supplementary Table II). Samples without template or reverse transcriptase served as negative controls. Expression levels were normalized to the housekeeping gene encoding glyceraldehyde-3-phosphate dehydrogenase (gapdh) obtained for every sample in parallel assays[15].

Human fetal NanoString analysis

Midgestational fetal brain subjects (18–22 weeks of gestation), collected after saline-induced elective abortions under Institutional Review Board approval at SUNY Downstate Medical Center, Brooklyn, New York, were fixed in 1% paraformaldehyde in 0.05M phosphate buffer for 24 h, frozen in dry ice-cooled isopentane, cryosectioned in the coronal plane (20 μm) and stored at −30 °C[62]. Tissue isolations from the cortex were carried out with micro-RNAqueous lysis solution (Life Technologies) and gene expression analyzed using the nCounter System from NanoString Technologies[63] at the Gene Expression Shared Resource Facility at Icahn School of Medicine. Briefly, the cell lysates were hybridized to a NanoString code-set containing barcode-labeled probes for ROBO1, SLIT1 and three housekeeping genes: TBP, Hsp90ab1 and ActB (Supplementary Table IV), followed by scanning of the immobilized mRNA transcripts in the nCounter Digital Analyzer. The raw data files were normalized to the TBP housekeeping gene (HKG) *via* NanoString nCounter software and statistical analysis was performed using the JMP statistical program (SAS Institute, Cary, NC). A general linear stepwise regression was used to calculate statistical significance and identify covariates. Variables were clustered as *i*) fetal age, *ii*) fetal body weight and foot length ("developmental measures") and *iii*) cannabis exposure. A univariate model was first performed with each cluster of variables and any variable that showed $p < 0.10$ was included in the stepwise regression in addition to cannabis exposure addition[62]. Variables with $p < 0.05$ were included in the final regression model as covariates of cannabis exposure.

Liquid chromatography tandem mass spectrometry

2-AG, anandamide (AEA), 2-linoleoyl glycerol (2-LG) and oleoyl ethanolamine (OEA) concentrations were determined using a solid-phase extraction liquid chromatography tandem mass spectrometry (LC-MS/MS) method[30,64]. The final JZL184 (40 mg/kg) injection was given to pregnant females on E18.5 2h before dissection of maternal and fetal brains. Embryonic hemisected brains ($n = 6$ pups from two separate litters) were homogenized in ice-cold acetonitrile containing $[^2H_4]$anandamide at 6 pmol as internal standard, made up to 70% water and centrifuged at 13,000 *rpm* for 5 min. The supernatant was applied to Strata-X polymeric reverse-phase cartridges (Phenomenex), methanol eluted analytes were dried under N_2, and the residue was re-suspended in mobile phase. A Surveyor LC system coupled to a TSQ Quantum mass spectrometer (Fisher Thermo Scientific) was used for analysis. The analytes were eluted from an ACE 5μ C8 column (150 × 2.1 mm; Hichrom Ltd.) under isocratic conditions with a mobile phase consisting of 15% water, 85% methanol, and 0.5% formic acid at a flow rate of 200 μl/min at 30 °C. Mass-spectrometry analysis was performed using electrospray ionization in positive ion mode. Quantification was undertaken using single-reaction monitoring of the parent ion-product ion transitions for 2-AG and $[^2H_4]$AEA of mass-to-charge ratio (m/z) of m/z 379 to m/z 287 and m/z 352.2 to m/z 66.2, respectively. Two peaks were present in the chromatogram for 2-AG because a 1(3)-isomer exists in equilibrium with 2-AG. The areas of both peaks were combined to calculate [2-AG] by weighted linear regression analysis against suitable calibration standards using Xcalibur 2.0.6 software (Fisher Thermo Scientific). Results were expressed as nmoles/pmoles per gram of tissue.

Ex vivo activity-based protein profiling

Frozen, hemisected brains from E18.5 mouse embryos (~35 mg; other hemisphere from mass spectrometry analysis) or a section of the cortex from the corresponding mother (~90 mg) were washed with cold DPBS (2 × 1.0 mL) and homogenized using a Branson Sonifier 250 probe sonicator (10 pulses, 50% duty cycle, output setting = 3.0) in cold DPBS (10 µl/mg tissue). Homogenates derived from adult mouse brain samples were centrifuged (3,000 g, 3 min) at 4 °C and the pellet was discarded. The total protein concentration for each tissue homogenate was then determined using the DC Protein Assay (Bio-Rad) and each proteome was diluted to 1.0 mg/mL in DPBS. Proteomes (50 µl) were subsequently treated with FP-Rhodamine (1.0 µl, 50 µM in DMSO), incubated for 30 min at room temperature and quenched with 4× SDS Loading Buffer (17 µl). Following separation of proteins by SDS-PAGE (10% acrylamide gel) and fluorescent gel imaging (Hitachi FMBio II flatbed scanner), serine hydrolase activities were determined by measuring the fluorescent intensity of target gel bands using ImageJ 1.45s[24].

Primary cultures, pharmacology and transfection

The pallium of embryonic mice was dissected at E16.5. For neuronal cultures, cortical cells from C57BL/6 and $CB_1R^{-/-}$ mice were enzymatically dissociated and plated at a density of 25-50,000 cells/well (morphometry) or 10^6 cells/well (biochemistry) in poly-D-lysine (PDL)-coated 24-well or 6-well plates, respectively[30]. Primary neuron cultures were maintained in DMEM/F12 (1:1) containing B27 supplement (2%), L-glutamine (2 mM), penicillin (100 U/ml), and streptomycin (100 µg/ml; all from Invitrogen) and exposed to drugs applied alone or in combination (JZL 184: 100nM, Cayman Chemical; O2050: 200nM, Tocris Bioscience; AM630: 200nM, Tocris Bioscience; AM251: 200nM, Tocris Bioscience; UO126: 10µM, Tocris Bioscience; SP600125: 5µM, Tocris Bioscience). Primary cortical neurons from C57BL6/N fetuses were transfected on 1 day *in vitro* by Lipofectamine 2000 (5 µl; Invitrogen) with a pool of MGL-specific siRNAs (sc-72278; 50 pmol/well) or non-targeting siRNA (sc-36869; 50pm/well; Santa Cruz Biotechnology) for 30 min. Neurons were left to recover for 3 days before fixation in 4% paraformaldehyde.

For glial cultures, neocortices of P2 mouse pups were dissected. Cells were dissociated similarly, transferred to T75 flasks (3×10^7 cells/flask) and maintained in DMEM containing 10% fetal bovine serum (FBS), L-glutamine (2 mM), penicillin (100 U/ml), and streptomycin (100 µg/ml). After 7-9 days, T75 flasks were placed on a shaker at 190 *rpm* at 37 °C for 1h. The microglial fraction was discarded and cells were allowed to equilibrate for 2 - 6h in fresh medium. Subsequently, flasks were placed onto an orbital shaker at 210 *rpm*, 37 °C for 16 - 18h to separate oligodendrocytes. The supernatant (oligodendroglial fraction) was collected, centrifuged, re-suspended and seeded at a density of 25,000 cells/well (morphometry) and 10^6 cells/well (biochemistry) in poly-D-lysine (PDL)-coated 24-well and 6-well plates, respectively. Cultures were then treated with JZL184 (100 nM) every other day for 72h or with MGL-specific siRNA/non-targeting siRNA as described above. Cell pellets from the same fraction were taken and processed for Western blotting and PCR analysis simultaneously. Astrocytes were collected in fresh medium and processed for protein and mRNA analysis.

For neuron-glia co-cultures, oligodendrocytes were plated at a density of 25,000 cells/well in DMEM containing 10% FBS. One day later, half of the medium was removed and replaced by DMEM/F12 (1:1) culture medium supplemented with B27 (2%) and neurons were seeded at a density of 25,000 cells/well. In another set of experiments, Lipofectamine 2000 (5 μl; Invitrogen) was used to transfect co-cultures with either non-targeting (scrambled) siRNA (sc-36869) or a pool of Robo1-specific mouse siRNAs (sc-42253; both at 100 pmol/well; Santa Cruz Biotechnology) for 4h. Co-cultures were treated with JZL184 (100 nM) every other day for 72h.

Cells on coverslips were immersion fixed on ice with 4% paraformaldehyde in 0.1M phosphate buffer and processed as above for immunocytochemistry. Morphological parameters were determined by analyzing calibrated images in the ZEN2010 imaging software module (Zeiss; $n > 30$ cells/group)[18,30]. In primary neuronal cultures, the intensity of Robo1 and Robo2 imunoreactivities along the neurite ($n > 20$ per marker and experimental group on two coverslips of two independent experiments each) was measured by obtaining a plot profile starting at the growth cone and continuing along the total axon back to the soma. In primary oligodendrocyte cultures, Slit2 immunoreactivity was measured in end-feet and along processes ($n > 30$ cells/group on two coverslips from duplicate experiments). Immunoreactivity was normalized to vehicle-treated end-feet. Distances between neurites and oligodendrocytes were measured in neuron-glia co-cultures ($n > 20$/ group on two coverslips from duplicates).

Growth cone particle isolation

Cortical hemispheres from E18.5 mouse embryos ($n = 5$ embryos/treatment) were vibratome sectioned (200-300 μm thickness), pooled ($n = 5$ embryos/treatment), and exposed to JZL184 (100 nM in DMEM/F12/B27 as above) for 25 or 80 minutes at 37°C *in vitro*. Control samples were incubated with vehicle for 80 min. Growth cone particles were isolated from vehicle or JZL184 treated samples according to published protocols[65]. Robo1 protein levels of growth cone particles were determined by Western blotting (Supplementary Table I). β-III-tubulin served as internal loading control[30].

Statistics

Data were analyzed using Statistical Package for the Social Sciences (version 21.0, SPSS Inc.). Pair-wise group comparisons in histochemical and Western blotting experiments were evaluated using Student's *t*-test (on independent samples). Data were normalized to controls as indicated. Data were expressed as means ± s.e.m. A *p* value of 0.05 was considered statistically significant.

Supplementary Material

Refer to Web version on PubMed Central for supplementary material.

ACKNOWLEDGEMENTS

REFERENCES

1. Brose K, et al. Slit proteins bind Robo receptors and have an evolutionarily conserved role in repulsive axon guidance. Cell. 1999; 96:795–806. [PubMed: 10102268]

2. Kolodkin AL, Tessier-Lavigne M. Mechanisms and molecules of neuronal wiring: a primer. Cold Spring Harb. Perspect. Biol. 2011; 3

3. Hohenester E. Structural insight into Slit-Robo signalling. Biochem. Soc. Trans. 2008; 36:251–256. [PubMed: 18363568]

4. Lopez-Bendito G, et al. Robo1 and Robo2 cooperate to control the guidance of major axonal tracts in the mammalian forebrain. J Neurosci. 2007; 27:3395–3407. [PubMed: 17392456]

5. Andrews W, et al. Robo1 regulates the development of major axon tracts and interneuron migration in the forebrain. Development. 2006; 133:2243–2252. [PubMed: 16690755]

6. Kadison SR, Murakami F, Matise MP, Kaprielian Z. The role of floor plate contact in the elaboration of contralateral commissural projections within the embryonic mouse spinal cord. Dev. Biol. 2006; 296:499–513.

7. Long H, et al. Conserved roles for Slit and Robo proteins in midline commissural axon guidance. Neuron. 2004; 42:213–223. [PubMed: 15091338]

8. Bagri A, et al. Slit proteins prevent midline crossing and determine the dorsoventral position of major axonal pathways in the mammalian forebrain. Neuron. 2002; 33:233–248. [PubMed: 11804571]

9. Kidd T, Bland KS, Goodman CS. Slit is the midline repellent for the robo receptor in Drosophila. Cell. 1999; 96:785–794. [PubMed: 10102267]

10. Simpson JH, Bland KS, Fetter RD, Goodman CS. Short-range and long-range guidance by Slit and its Robo receptors: a combinatorial code of Robo receptors controls lateral position. Cell. 2000; 103:1019–1032. [PubMed: 11163179]

11. Rajagopalan S, Nicolas E, Vivancos V, Berger J, Dickson BJ. Crossing the midline: roles and regulation of Robo receptors. Neuron. 2000; 28:767–777. [PubMed: 11163265]

12. Plump AS, et al. Slit1 and Slit2 cooperate to prevent premature midline crossing of retinal axons in the mouse visual system. Neuron. 2002; 33:219–232. [PubMed: 11804570]

13. Nguyen Ba-Charvet KT, et al. Slit2-Mediated chemorepulsion and collapse of developing forebrain axons. Neuron. 1999; 22:463–473. [PubMed: 10197527]

14. Ypsilanti AR, Zagar Y, Chedotal A. Moving away from the midline: new developments for Slit and Robo. Development. 2010; 137:1939–1952. [PubMed: 20501589]

15. Berghuis P, et al. Endocannabinoids regulate interneuron migration and morphogenesis by transactivating the TrkB receptor. Proc. Natl. Acad. Sci. U. S. A. 2005; 102:19115–19120. [PubMed: 16357196]

16. Aguado T, et al. The endocannabinoid system promotes astroglial differentiation by acting on neural progenitor cells. J. Neurosci. 2006; 26:1551–1561. [PubMed: 16452678]

17. Wu CS, et al. Requirement of cannabinoid CB(1) receptors in cortical pyramidal neurons for appropriate development of corticothalamic and thalamocortical projections. Eur. J. Neurosci. 2010; 32:693–706. [PubMed: 21050275]

18. Mulder J, et al. Endocannabinoid signaling controls pyramidal cell specification and long-range axon patterning. Proc. Natl. Acad. Sci. U. S. A. 2008; 105:8760–8765. [PubMed: 18562289]

19. Berghuis P, et al. Hardwiring the brain: endocannabinoids shape neuronal connectivity. Science. 2007; 316:1212–1216. [PubMed: 17525344]

20. Molina-Holgado E, et al. Cannabinoids promote oligodendrocyte progenitor survival: involvement of cannabinoid receptors and phosphatidylinositol-3 kinase/Akt signaling. J. Neurosci. 2002; 22:9742–9753. [PubMed: 12427829]

21. Gomez O, et al. The constitutive production of the endocannabinoid 2-arachidonoylglycerol participates in oligodendrocyte differentiation. Glia. 2010; 58:1913–1927. [PubMed: 20878765]

22. De Robertis E, Gerschenfeld HM, Wald F. Cellular mechanism of myelination in the central nervous system. J Biophys. Biochem. Cytol. 1958; 4:651–656. [PubMed: 13587562]

23. Schlosburg JE, et al. Chronic monoacylglycerol lipase blockade causes functional antagonism of the endocannabinoid system. Nat. Neurosci. 2010; 13:1113–1119. [PubMed: 20729846]

24. Long JZ, et al. Selective blockade of 2-arachidonoylglycerol hydrolysis produces cannabinoid behavioral effects. Nat. Chem. Biol. 2009; 5:37–44. [PubMed: 19029917]

25. Cravatt BF, et al. Molecular characterization of an enzyme that degrades neuromodulatory fatty-acid amides. Nature. 1996; 384:83–87. [PubMed: 8900284]

26. Wolfer DP, Henehan-Beatty A, Stoeckli ET, Sonderegger P, Lipp HP. Distribution of TAG-1/axonin-1 in fibre tracts and migratory streams of the developing mouse nervous system. J. Comp Neurol. 1994; 345:1–32. [PubMed: 8089271]

27. Denaxa M, Chan CH, Schachner M, Parnavelas JG, Karagogeos D. The adhesion molecule TAG-1 mediates the migration of cortical interneurons from the ganglionic eminence along the corticofugal fiber system. Development. 2001; 128:4635–4644. [PubMed: 11714688]

28. Molnar Z, Blakemore C. How do thalamic axons find their way to the cortex? Trends Neurosci. 1995; 18:389–397. [PubMed: 7482804]

29. Tucker KL, Meyer M, Barde YA. Neurotrophins are required for nerve growth during development. Nat. Neurosci. 2001; 4:29–37. [PubMed: 11135642]

30. Keimpema E, et al. Differential subcellular recruitment of monoacylglycerol lipase generates spatial specificity of 2-arachidonoyl glycerol signaling during axonal pathfinding. J. Neurosci. 2010; 30:13992–14007. [PubMed: 20962221]

31. Luxardi G, et al. Glypicans are differentially expressed during patterning and neurogenesis of early mouse brain. Biochem. Biophys. Res. Commun. 2007; 352:55–60. [PubMed: 17107664]

32. Friedlander DR, et al. The neuronal chondroitin sulfate proteoglycan neurocan binds to the neural cell adhesion molecules Ng-CAM/L1/NILE and N-CAM, and inhibits neuronal adhesion and neurite outgrowth. J Cell Biol. 1994; 125:669–680. [PubMed: 7513709]

33. Bisogno T, et al. Cloning of the first sn1-DAG lipases points to the spatial and temporal regulation of endocannabinoid signaling in the brain. J. Cell Biol. 2003; 163:463–468. [PubMed: 14610053]

34. Blankman JL, Simon GM, Cravatt BF. A comprehensive profile of brain enzymes that hydrolyze the endocannabinoid 2-arachidonoylglycerol. Chem. Biol. 2007; 14:1347–1356. [PubMed: 18096503]

35. Marrs WR, et al. The serine hydrolase ABHD6 controls the accumulation and efficacy of 2-AG at cannabinoid receptors. Nat. Neurosci. 2010; 13:951–957. [PubMed: 20657592]

36. Straiker A, Min KT, Mackie K. Fmr1 deletion enhances and ultimately desensitizes CB1 signaling in autaptic hippocampal neurons. Neurobiol. Dis. 2013; 56:1–5. [PubMed: 23578490]

37. Rothberg JM, Jacobs JR, Goodman CS, rtavanis-Tsakonas S. slit: an extracellular protein necessary for development of midline glia and commissural axon pathways contains both EGF and LRR domains. Genes Dev. 1990; 4:2169–2187. [PubMed: 2176636]

38. Carmeliet P, Tessier-Lavigne M. Common mechanisms of nerve and blood vessel wiring. Nature. 2005; 436:193–200. [PubMed: 16015319]

39. Hivert B, Liu Z, Chuang CY, Doherty P, Sundaresan V. Robo1 and Robo2 are homophilic binding molecules that promote axonal growth. Mol. Cell Neurosci. 2002; 21:534–545. [PubMed: 12504588]

40. Ortar G, et al. Tetrahydrolipstatin analogues as modulators of endocannabinoid 2-arachidonoylglycerol metabolism. J Med. Chem. 2008; 51:6970–6979. [PubMed: 18831576]

41. Keimpema E, Mackie K, Harkany T. Molecular model of cannabis sensitivity in developing neuronal circuits. Trends Pharmacol. Sci. 2011; 32:551–561. [PubMed: 21757242]

42. Andrews W, et al. The role of Slit-Robo signaling in the generation, migration and morphological differentiation of cortical interneurons. Dev. Biol. 2008; 313:648–658. [PubMed: 18054781]

43. Argaw A, et al. Concerted action of CB1 cannabinoid receptor and deleted in colorectal cancer in axon guidance. J. Neurosci. 2011; 31:1489–1499. [PubMed: 21273433]

44. Kinrade EF, Hidalgo A. Lateral neuron--glia interactions steer the response of axons to the Robo code. Neuron Glia Biol. 2004; 1:101–112. [PubMed: 18273400]

45. Buckley NE, Hansson S, Harta G, Mezey E. Expression of the CB1 and CB2 receptor messenger RNAs during embryonic development in the rat. Neuroscience. 1998; 82:1131–1149. [PubMed: 9466436]

46. Berrendero F, Sepe N, Ramos JA, Di Marzo V, Fernandez-Ruiz JJ. Analysis of cannabinoid receptor binding and mRNA expression and endogenous cannabinoid contents in the developing rat brain during late gestation and early postnatal period. Synapse. 1999; 33:181–191. [PubMed: 10420166]

47. Diaz-Alonso J, et al. The CB1 cannabinoid receptor drives corticospinal motor neuron differentiation through the Ctip2/Satb2 transcriptional regulation axis. J Neurosci. 2012; 32:16651–16665. [PubMed: 23175820]

48. Keimpema E, et al. Diacylglycerol lipase alpha manipulation reveals developmental roles for intercellular endocannabinoid signaling. Sci. Rep. 2013; 3:2093. [PubMed: 23806960]

49. Wilson RI, Nicoll RA. Endogenous cannabinoids mediate retrograde signalling at hippocampal synapses. Nature. 2001; 410:588–592. [PubMed: 11279497]

50. Yang L, Bashaw GJ. Son of sevenless directly links the Robo receptor to rac activation to control axon repulsion at the midline. Neuron. 2006; 52:595–607. [PubMed: 17114045]

51. Wong K, et al. Signal transduction in neuronal migration: roles of GTPase activating proteins and the small GTPase Cdc42 in the Slit-Robo pathway. Cell. 2001; 107:209–221. [PubMed: 11672528]

52. Yuan XB, et al. Signalling and crosstalk of Rho GTPases in mediating axon guidance. Nat. Cell Biol. 2003; 5:38–45. [PubMed: 12510192]

53. Huizink AC, Mulder EJ. Maternal smoking, drinking or cannabis use during pregnancy and neurobehavioral and cognitive functioning in human offspring. Neurosci. Biobehav. Rev. 2006; 30:24–41. [PubMed: 16095697]

54. Huizink AC. Prenatal cannabis exposure and infant outcomes: Overview of studies. Prog. Neuropsychopharmacol. Biol. Psychiatry. 2013

55. Keimpema E, Mackie K, Harkany T. Molecular model of cannabis sensitivity in developing neuronal circuits. Trends Pharmacol. Sci. 2011; 32:551–561. [PubMed: 21757242]

56. Bambang KN, et al. Immunity and early pregnancy events: are endocannabinoids the missing link? J Reprod. Immunol. 2012; 96:8–18. [PubMed: 23177537]

57. Yeh ML, et al. Robo1 Modulates Proliferation and Neuogenesis in the Developing Neocortex. J Neurosci. 2014

58. Lendvai D, et al. Neurochemical mapping of the human hippocampus reveals perisynaptic matrix around functional synapses in Alzheimer's disease. Acta Neuropathol. 2013; 125:215–229. [PubMed: 22961619]

59. Kanaumi T, Milenkovic I, dle-Biassette H, Aronica E, Kovacs GG. Non-neuronal cell responses differ between normal and Down syndrome developing brains. Int. J. Dev. Neurosci. 2013; 31:796–803. [PubMed: 24113258]

60. Iyer A, et al. Developmental patterns of DR6 in normal human hippocampus and in Down syndrome. J. Neurodev. Disord. 2013; 5:10. [PubMed: 23618225]

61. Bradford MM. A rapid and sensitive method for the quantitation of microgram quantities of protein utilizing the principle of protein-dye binding. Anal. Biochem. 1976; 72:248–254. [PubMed: 942051]

62. Hurd YL, et al. Marijuana impairs growth in mid-gestation fetuses. Neurotoxicol. Teratol. 2005; 27:221–229.

63. Geiss GK, et al. Direct multiplexed measurement of gene expression with color-coded probe pairs. Nat. Biotechnol. 2008; 26:317–325. [PubMed: 18278033]

64. Giuffrida A, Rodriguez de FF, Piomelli D. Quantification of bioactive acylethanolamides in rat plasma by electrospray mass spectrometry. Anal. Biochem. 2000; 280:87–93. [PubMed: 10805525]

65. Lockerbie RO, Miller VE, Pfenninger KH. Regulated plasmalemmal expansion in nerve growth cones. J. Cell Biol. 1991; 112:1215–1227. [PubMed: 1999470]
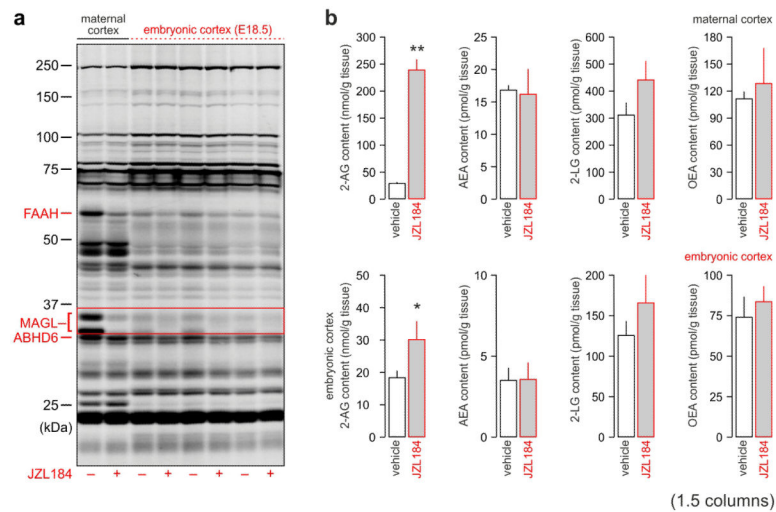
Fig. 1.

JZL184 increases 2-AG levels in maternal and embryonic brains. (**a**) *Ex vivo* activity-based protein profiling of brain-derived serine hydrolases in vehicle and JZL184 (40 mg/kg)-treated adult and fetal cortices. (**b**) Select 2-monoacyl glycerol and *N*-acyl amide levels in maternal and fetal brains correlatively measured after JZL184 treatment. Data were expressed as means ± s.e.m., $n = 2$/group (mothers), $n = 6$/group (fetuses); **$p < 0.01$, *$p < 0.05$ (Student's *t*-test).
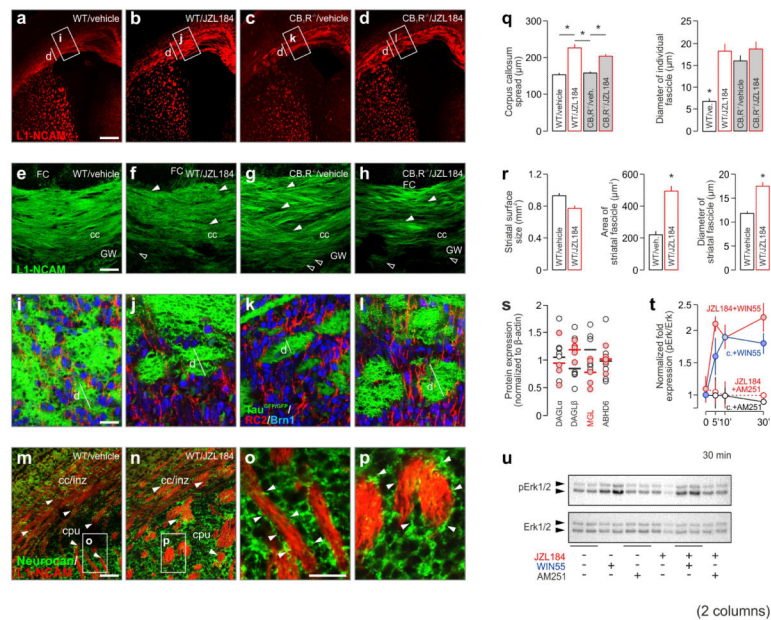
(2 columns)

Fig. 2.
JZL184 alters callosal axon fasciculation and pathfinding. (**a-d**) Corticofugal axonal phenotypes and (**b-h**) their midline crossing in vehicle or JZL184-treated mouse embryos at E18.5. (**i-l**) A tau[gfp/gfp] reporter mouse[29] was used for the genetic tagging of corticofugal axons.. Axon fasciculation errors present in $CB_1R^{-/-}$ mice (**k**), were further increased by JZL184 (surface area occupied by corticofugal axons (**l**). (**m-p**) Neurocan was excluded from enlarged axon fascicles in JZL184-exposed brains. (**q**) Corpus callosum spread in both wild-type and $CB_1R^{-/-}$ mice. (**r**) Striatal surface size, and the cross-sectional surface area and diameter of axon fascicles in JZL184– or vehicle-treated mice. (**s**) DAGLα, DAGLβ, MGL and ABHD6 protein levels in JZL184-treated (*red circles*) *vs*. control (*open circles*) cortices on E18.5. (**t,u**) Erk1/2 phosphorylation upon acute WIN55,212-2 and/or AM251 stimulation in drug naive and JZL184 pre-treated (4 days) neurons. Data were expressed as means ± s.e.m., *n* = 3/group (**q,r**). In vitro experiments were performed in duplicates with n 2 samples/experiments run in parallel. *p < 0.05 (Student's *t*-test). *Scale bars* = 300 μm (a-h, m,n), 10 μm (i-l,o,p).
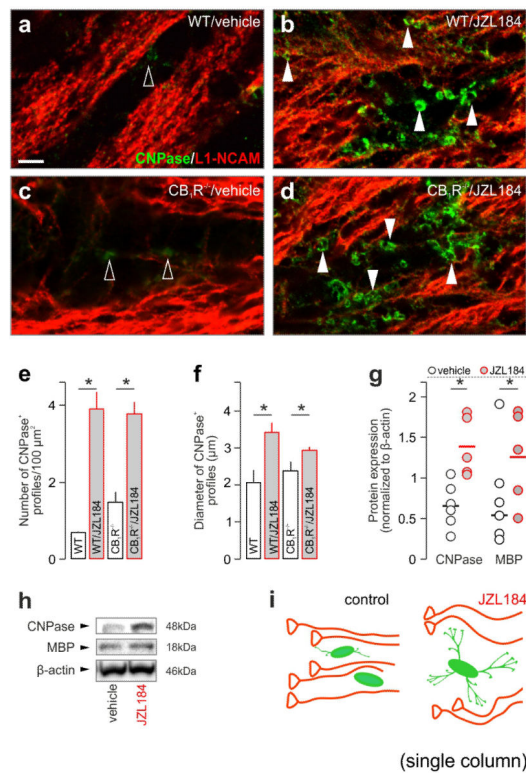
Fig. 3.
JZL184 induces oligodendrocyte differentiation. CNPase[+] oligodendroyctes in the prospective corpus callosum were infrequently detected in wild-type (**a**) and $CB_1R^{-/-}$ (**c**) embryos (E18.5; *open arrowheads*). (**b,d**) JZL184-induced oligodendrocyte differentiation, which progressed in $CB_1R^{-/-}$ mice (*solid arrowheads* pinpoint end-feet). (**e,f**) Quantitative data on oligodendrocyte morphology. (**g,h**) CNPase and MBP levels in the cortices of JZL184-treated mouse embryos. (**i**) Schema of JZL184-induced remodeling of axonal pathfinding upon premature oligodendrocyte differentiation. Data were expressed as means ± s.e.m., n = 5/6 (JZL184/vehicle), *$p < 0.05$ (Student's *t*-test). *Scale bar* = 4 μm (a).
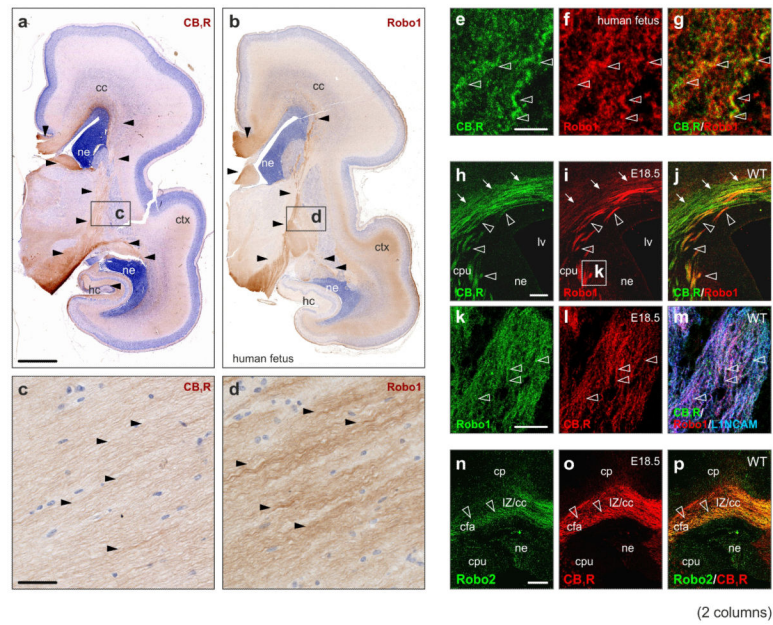
Fig. 4.
CB$_1$Rs co-localize with Robo1 receptors in human and mouse corticofugal axons. (**a,b**) The regional distribution of CB$_1$R and Robo1 receptor immunoreactivities in human fetal serial sections (*closed arrowheads*). (**c,d**) CB$_1$R and Robo1 receptor immunoreactivities in corticofugal fibers in the internal capsule at high-magnification. (**e-g**) Co-localization of CB$_1$R and Robo1 receptors in human fetal tissues (internal capsule) by high-resolution laser scanning microscopy (*open arrowheads*). Robo1 (**h-m**), as well as Robo2 (**n-p**), was co-expressed with CB$_1$Rs in mouse callosal axons (*arrowheads*). *Abbreviations:* cc, corpus callosum; cfa, corticofugal axons; cp, cortical plate; cpu, caudate putamen; hc, hippocampus; IZ, intermediate zone; ne, neuroepithelium. *Scale bars* = 3mm (a), 200 μm (h,n), 40 μm, (c), 7 μm (k).
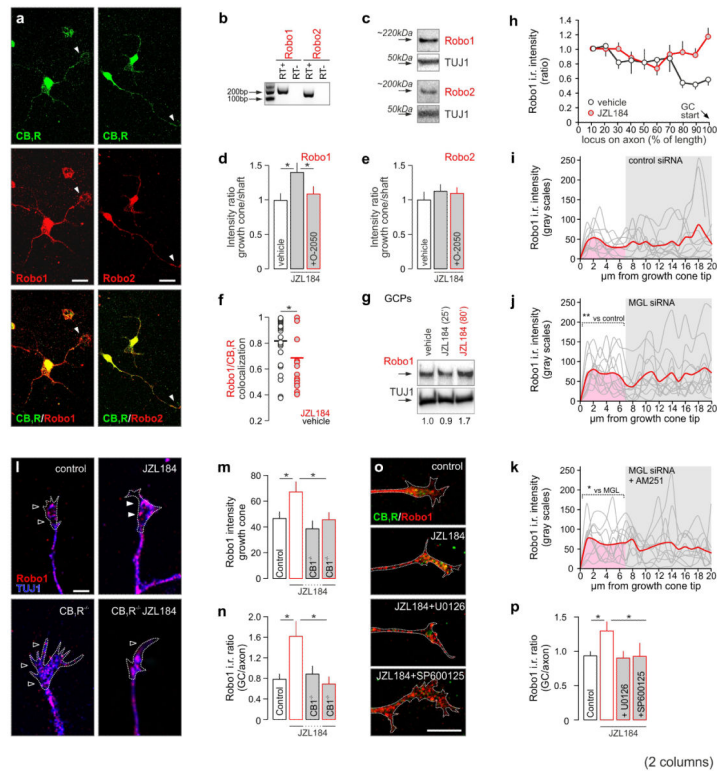
Fig. 5.
CB$_1$R stimulation regulates subcellular Robo1 positioning. (**a**) Robo1 and Robo2 immunoreactivity in the somata and neurites (including growth cone; *arrowheads*) of CB$_1$R$^+$ cortical neurons *in vitro*. (**b,c**) Cultured cortical neurons expressed both Robo1/Robo2 mRNA and protein. (**d**) Robo1 and Robo2 (**e**), fluorescence intensity in growth cones treated with JZL184 or O-2050, a CB$_1$R antagonist. (**f**) Co-localization coefficient of Robo1 and CB$_1$R in growth cones upon JZL184 exposure. (**g**) JZL184 induced Robo1 accumulation in growth cones *ex vivo* in isolated growth cone particles (GCPs). (**h**) Robo1 immunoreactivity adjacent to the growth cone in JZL184 treated neurons. (**i-k**) Robo1 immunoreactivity in growth cones upon siRNA-mediated MGL silencing in cultured primary neurons. (**l-n**) Effect of the genetic ablation of CB$_1$Rs in cortical neurons on Robo1 receptor expression in growth cones after JZL184 or vehicle administration. (**o,p**) The effect of Erk1/2 (U0126) and JNK1 (SP600125) inhibition on Robo1 distribution. Data were expressed as means ± s.e.m., from triplicate experiments (sample size: 8-25 neurons/group in morphometric analysis), $*p < 0.05$ (Student's *t*-test). *Scale bars* = 10 μm (a), 5 μm (l,o).
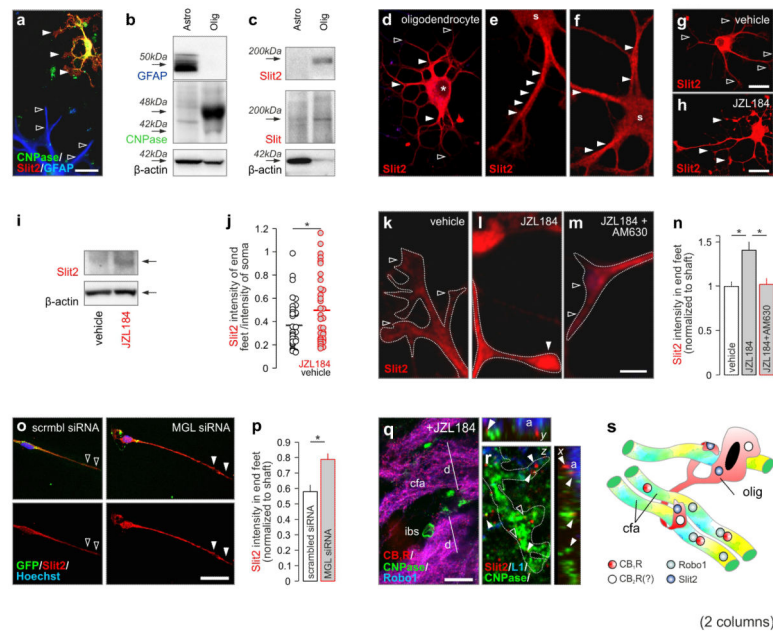
Fig. 6.

JZL184 alters Slit2 expression and localization in oligodendrocytes. (**a**) Oligodendrocytes (*solid arrowheads*), but not astrocytes, (*open arrowheads*) contained Slit2. (**b**) GFAP and CNPase were used to validate the purity of isolated astrocytes and oligodendrocytes, respectively. (**c**) Oligodendrocytes, but not astrocytes, contained mature Slit2. An additional antibody raised against a phylogenetically conserved epitope of *Drosophila* Slit confirmed this finding (*Slit*). (**d-f**) Slit2-like immunoreactivity localized to oligodendrocyte somas (*s*) and processes. Membranous staining pattern is shown in both e and f (*arrowheads*). Asterisks (*) indicate location of the nucleus. (**g,h**) Oligodendrocyte differentiation and increased Slit2 immunoreactivity, particularly in end-feet (*arrowheads*), upon JZL184 exposure. (**i**) Slit2 protein content in oligodendrocytes after JZL184 treatment. (**j**) JZL184-induced Slit2 accumulation in oligodendrocyte end-feet as measured by quantitative morphometry. (**k-k**) Effect of AM630, a CB_2R antagonist, on JZL184-induced Slit2 accumulation in oligodendrocyte end-feet (*open and closed arrowheads*). (**o,p**) The effect of siRNA-mediated MGL inhibition on Slit2 expression in end-feet (*arrowheads*). (**q**) CNPase[+] oligodendroglial end-feet in the interbundle space (ibs) and in apposition to enlarged fascicles of Robo1^{+} corticofugal axons (cfa) in JZL184-treated mouse embryos. (**r**) Three-dimensional reconstruction of Slit2 in oligodendrocyte end-feet (*arrowheads*) adjacent to corticofugal axons. (**s**) Schematic of JZL184-induced remodeling of axonal pathfinding upon premature oligodendrocyte differentiation. Data were expressed as means ± s.e.m., $n = 8 - 32$ cells/group for each condition in duplicate experiments; *$p < 0.05$ (Student's *t*-test). *Scale bars* = 10 μm (a,h,o,q), 2 μm (m).

(2 columns)
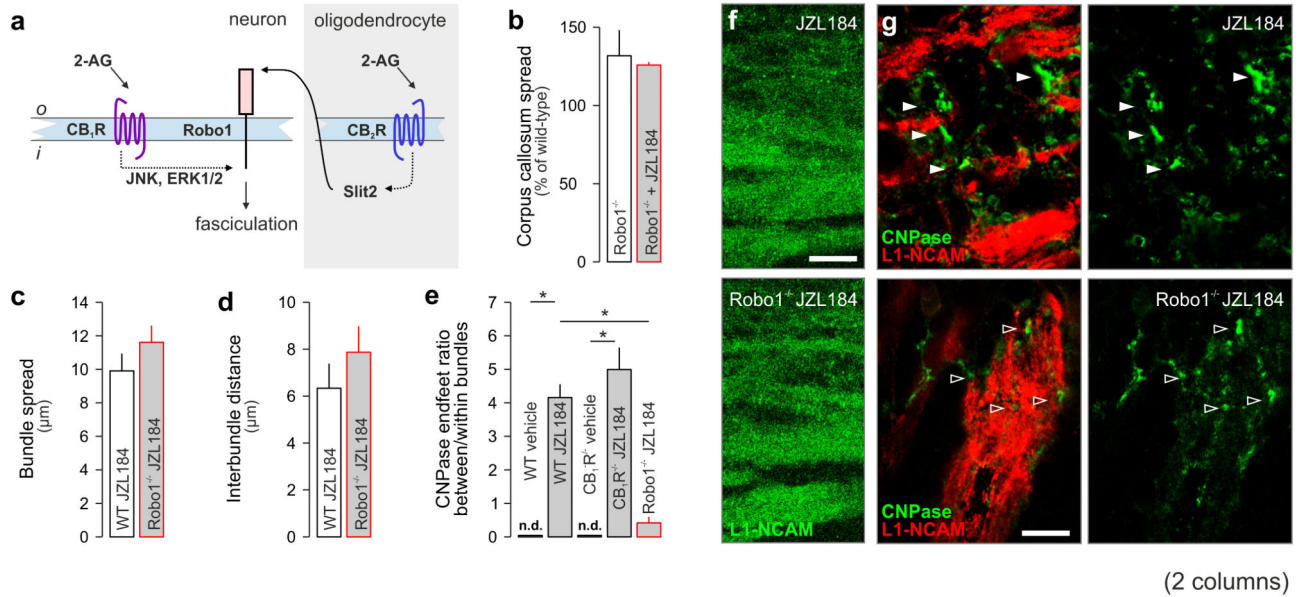
Fig. 7.

JZL184-induced oligodendroglial repositioning in Robo1$^{-/-}$ mice. (**a**) Schematic overview of 2-AG signaling converging on axonal growth and fasciculation through Slit/Robo signaling. (**b**) Callosal axon fasciculation in Robo1$^{-/-}$ mice treated with JZL184. Note that untreated Robo1$^{-/-}$ mice presented a fasciculation phenotype[5]. (**c,d**) Diameter of individual bundles and their interbundle distance upon JZL184 treatment in Robo1$^{-/-}$ embryos. (**e-g**) Oligodendroglia end-feet infiltrated axonal bundles in JZL184-treated Robo1$^{-/-}$ mice. This was undetected (n.d.) in wild-type or CB$_1$R$^{-/-}$ embryos. Data were expressed as means ± s.e.m., from n = 3-5 embryos/genotype; *$p < 0.05$ *vs*. respective wild-type (WT) controls (Student's *t*-test). *Scale bars* =10 μm (f,g).

(2 columns)
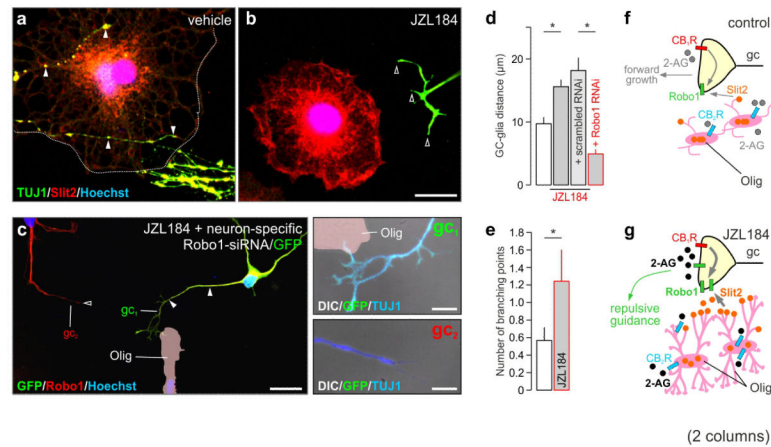
Fig. 8.
JZL184 induces growth cone repulsion *via* Slit2/Robo1 signaling. (**a**) Neurites (*arrowheads*) contacting oligodendrocytes when co-cultured. (**b**) Neurites (*open arrowheads*) excluded from the vicinity of oligodendrocytes upon JZL184 application. Note the intensely Slit2$^+$ peripheral domain of the oligodendrocyte (Olig) shown. (**c**) A neurite (*arrowheads*) of a Robo1 siRNA/GFP co-transfected neuron (gc_1 in green), but not of a non-transfected neuron (gc_2 in red), overcame chemorepulsion. Insets (gc_1,gc_2) depict high-resolution images of the growth cones shown in (**c**). (**d**) Growth cone distances to the most proximal surface of the nearest oligodendrocyte. (**e**) JZL184 induced branching of neuronal processes in the vicinity of oligodendrocytes *in vitro*. (**f,g**) Schema of Slit2/Robo1 signaling downstream from cannabinoid receptors. Data were expressed as means ± s.e.m., triplicate experiments with *n* = 3 samples run in parallel; *n* = 6-9 observations/group. *$p < 0.05$ (Student's *t*-test). *Scale bars* = 8 μm (a_1,b), 3 μm (insets).